Anisotropy of additively manufactured Ti-6-4 lattice structure

Cite as: AIP Conference Proceedings **2176**, 020002 (2019); https://doi.org/10.1063/1.5135114
Published Online: 19 November 2019

Yu. N. Loginov, S. I. Stepanov, I. A. Naschetnikova, and G. Muller-Kamskii

Anisotropy of Additively Manufactured Ti-6-4 Lattice Structure

Yu. N. Loginov[1, a)], S. I. Stepanov[1, b)], I. A. Naschetnikova[1, c)], and G. Muller-Kamskii[2, d)]

[1]*B. N. Yeltsin Ural Federal University, 19 Mira St., Ekaterinburg, 620002, Russia*
[2]*Israel Institute of Metals, Technion R&D Foundation, 3200003 Technion City, Haifa, Israel*

[a)]Corresponding author: yu.n.loginov@urfu.ru
[b)]Corresponding author: s.i.stepanov@urfu.ru
[c)]naschetnikova@mail.ru
[d)]garym@trdf.technion.ac.il

Abstract. Selective laser melting (SLM) is an additive manufacturing technique, where several aspects resulting in the anisotropy of properties is combined. This study provides an analysis of selective laser melting of the diamond lattice structure of Ti-6Al-4 in terms of anisotropy of Vickers microhardness depending on the location and direction of indentation. A statistical review of microhardness values is presented.

INTRODUCTION

The use of 3D-printing for metals makes it possible to produce parts with complex configurations [1], including structurally heterogeneous cellular structures used for orthopedic implants [2, 3]. The employment of metal powders in additive manufacturing has some features compared to their utilization as raw materials in conventional powder metallurgy. In traditional methods of powder metallurgy, it is necessary, firstly, to give the powder the shape of the product and then subject the preform to a liquid- or solid-phase sintering. It is possible to obtain anisotropy of product properties since, when the powder is compressed, one of the strain tensor components will be larger than the others. For example, during compression in a cylindrical mold, shortening will appear only in the direction of the punch motion, and it will be equal to zero in the other directions of deformation. This results in the heredity of the form of pores and, therefore, in the anisotropy of the mechanical properties of the product. The similar question of anisotropy in a powder medium arises for laser fusion technologies. The purpose of this study is to investigate the anisotropy of properties caused by the directivity of laser powder bed fusion.

TECHNOLOGY ANALYSIS

In laser powder bed fusion, parts are built up additively, layer by layer, due to selective melting of the powder. Thus, the direction of thermal action is already set in the kinematics of the process, which should affect the properties of an as-built part. The diagrams in Fig. 1 illustrate the foregoing as follows: the horizontal lines demonstrate the distribution of the powder layers, and the arrows indicate the direction of laser beam displacement. When the beam moves unidirectionally (Fig. 1a) along the x axis, a deliberately unidirectional thermal effect on the powder is implemented, which results in an anisotropic structure. This effect is complicated by the return of the beam along an adjacent trajectory, with a change in the direction by 180°. This method is termed zigzag hatching [4]. However, the anisotropy along the x-direction still occurs. To avoid this, multidirectional beam motion in the xy plane is usually employed due to a change in the direction of hatching from layer to layer (Fig. 1b). The angle between the hatching directions of adjacent layers may vary, but it generally is 90°.

Mechanics, Resource and Diagnostics of Materials and Structures (MRDMS-2019)
AIP Conf. Proc. 2176, 020002-1–020002-4; https://doi.org/10.1063/1.5135114
Published by AIP Publishing. 978-0-7354-1923-0/$30.00

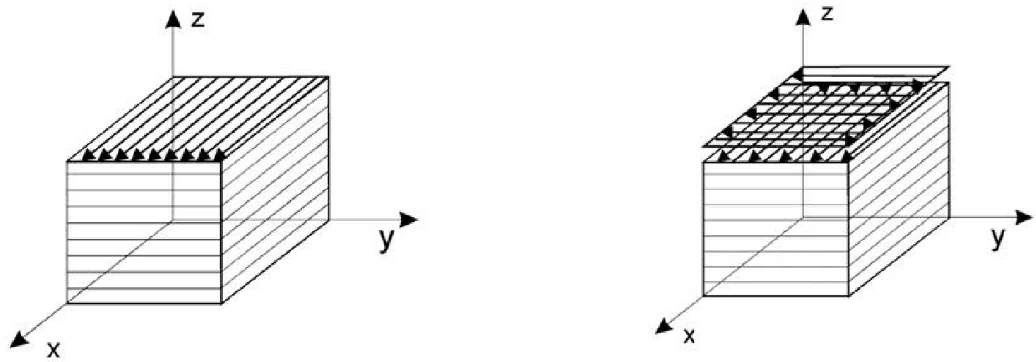

(a) (b)

FIGURE 1. Scheme of SLM scanning strategies: unidirectional along *x* (a); changing directions along the *x* and *y* axes from layer to layer (b)

As can be seen from Fig. 1, it is possible to equalize the thermal effect only in the *xy*-plane. In the *z*-direction, the powder is layered, each layer being melted only after the formation of the previous layer. This creates conditions for the development of an inhomogeneous metal structure, which can result in the anisotropy of the finished part. The foregoing applies to the production of both solid products and products with a cellular or lattice structure.

METHODS AND DISCUSSION

To evaluate the anisotropy of the properties of metallic material manufactured by 3D printing, lattice-structured Ti-6Al-4V ELI ($\alpha+\beta$)-titanium alloy samples were selected. According to the matweb.com website, the chemical composition of the alloy is as follows (wt.%): Al 5.5–6.5, V 3.5–4.5, C ≤0.080, H ≤0.0125, Fe ≤0.25, N ≤0.030, O ≤0.13, with the total impurity content of ≤0.40 and a content of each impurity of ≤0.10. The prefix ELI (Extra Low Interstitial) means more stringent restrictions on the impurities [5]; such materials are recommended for medical applications. The architectural design of the lattice structure corresponded to the diamond crystal lattice, which is often used in the 3D-printing technology [6, 7]. The unit cell is represented as a system of cylindrical struts oriented at an angle of 109°28′ to each other. The samples were manufactured by selective laser melting (SLM) using an EOSINT 280. The diamond lattice is demonstrated in Fig. 2a, and the build direction corresponds to the *z*-axis from the bottom up.

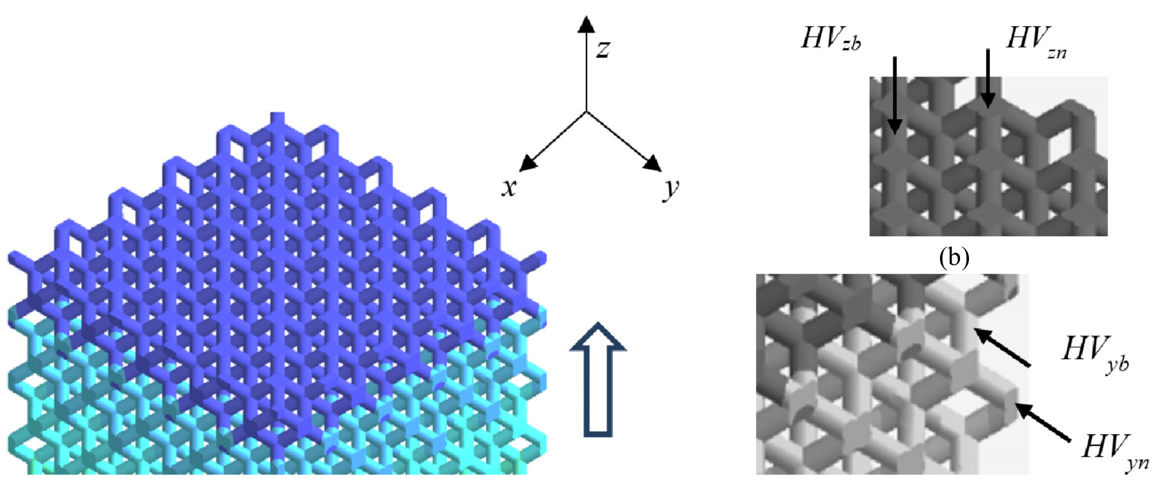

(a) (c)

FIGURE 2. Design of the lattice structure in *xyz*-coordinates (a). The build direction (BD) is indicated with a white arrow in a general view. The indentation direction is indicated with black arrows: top view (b) and side view (c)

The fragments of the upper and lateral parts of the lattice structure are shown in Fig. 2b and 2c respectively. The black arrows indicate the locations and directions of the HV microhardness measurement. The following subscripts were introduced: *y* and *z* show the direction of measurement along the corresponding coordinate axis, *b* shows the measurement location in the zone of the beam or the strut, and *n* indicates the measurement location in the zone of the node of adjacent struts.

The samples for measuring the HV microhardness were separated by using an electrical discharge machine followed by mounting into conductive plastic, grinding on SiC paper, and polishing with Struers OP-S NonDry colloidal silica. Microindentation was carried out on a CSM ConScan equipped with a Vickers indenter under a load of 9 N. The indentations are indicated in Fig. 3 with arrows. In the figure, the white background is the surface of the metal and the gray background is the surface of the mounting. The distance between the indentations is greater than four times the diagonal size, as well as the distance from the outer side of the sample, so that the measurements were carried out correctly.

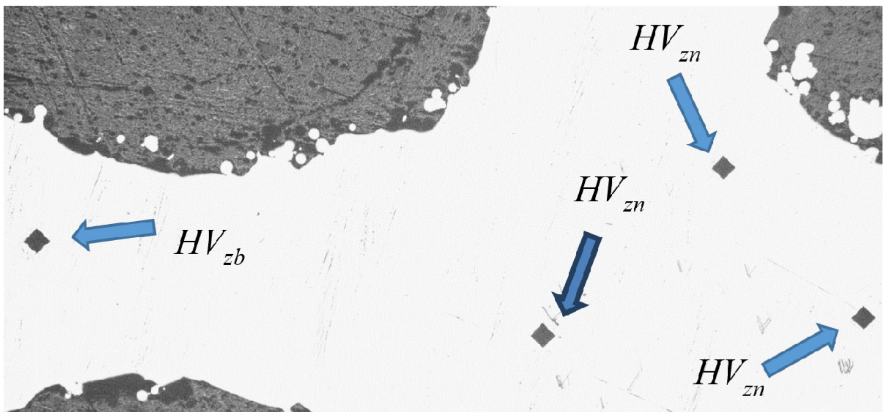

FIGURE 3. A magnified image of the struts of the additively manufactured lattice structure with square-shaped indentations indicated as HVzb for the struts (beams) and HVzn for the nodes of the struts

The number of indentations was 12 for each of the four zones determined above. Average values and dispersions were calculated. The results are shown in the form of diagrams in Figs. 4 and 5.

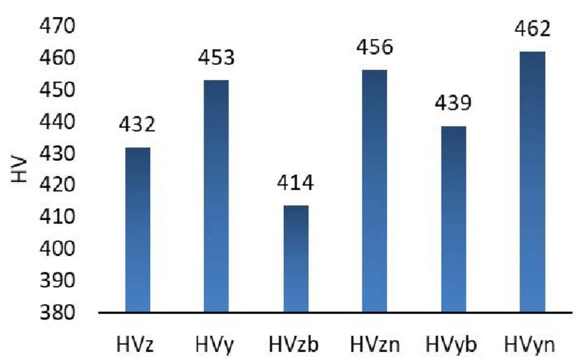

FIGURE 4. Vickers microhardness depending on the direction and location of indentation

The average microhardness value for all types of measurements was 443 HV. The microhardness measurements performed earlier without taking into account the location and direction of measurements demonstrated 420 HV for the as-built alloy [8]. These data agree well with the above. Other studies for the same alloy may provide lower values of microhardness, e.g. 360 HV in [9]; this is attributable to the increased porosity of the metal (up to 1%), as well as the SLM parameters. The values of HVy and HVz are averaged for the measurement directions along the y and z axes, regardless of the measurement location. It follows from comparison that, on the sites of the lateral surface, the hardness is approximately 5% higher than in the build direction. The effect of the reduced strength of a titanium alloy in the printing direction was noted in previous studies [10].

When specific regions are considered, the hardness of the beam/strut is lower than in the node of the struts. The lowest microhardness was found for the strut in the z build direction.

Structurally inhomogeneous samples are characterized by property fluctuations. Therefore, microhardness dispersion plots are given for the considered measurement (Fig. 5).

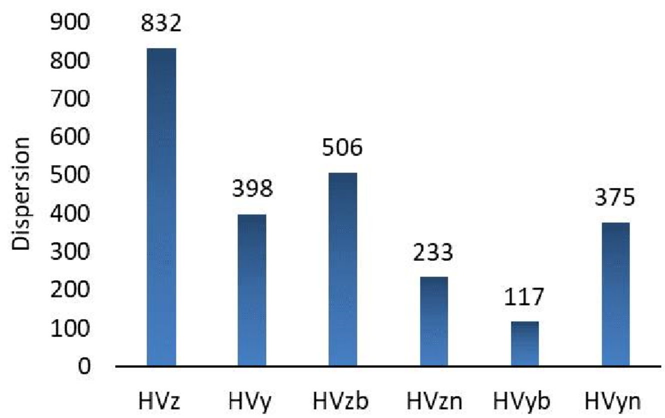

FIGURE 5. Dispersion of Vickers microhardness in various regions of the lattice structure

It can be seen that the highest dispersion is observed for measurements along the *z*-axis, i.e. in the build direction. The main contribution is made by microhardness distribution in the body of struts. In the transverse *y*-direction, the total dispersion is twice as high, and it is more provided by the nodes of the lattice. This is attributable to the fact that the hatching distance used (transverse motion of the laser beam) proved to be too large, and this led to the effect of inhomogeneous properties.

CONCLUSION

Relationships between the properties of titanium alloy in certain directions during 3D printing have been established. The microhardness has been shown to be approximately 5% higher in the lateral surface than in the build direction surface. The greatest dispersion of the microhardness number is characteristic of the build direction for selective laser melting.

ACKNOWLEDGMENTS

We hereby acknowledge the support of the Ministry of Education and Science of the Russian Federation, in accordance with the decree of the Government of April 9, 2010, No. 218, project No. 03.G25.31.0234.

REFERENCES

1. E. Bassoli, A. Gatto, L. Iuliano, and M.G. Violante, Rapid Prototyping Journal **13** (3), 148–155 (2007).
2. M. Elsayed, M. Ghazy, Y. Youssef, and K. Essa, Rapid Prototyping Journal **25** (3), 433–447 (2019).
3. Y. Loginov, S. Stepanov, and E. Khanykova, Solid State Phenomena **265**, 606–610 (2017).
4. L. Thijs, F. Verhaeghe, T. Craeghs, J. V. Humbeeck, and J.-P. Kruth, Acta Materialia **58**, 3303–3312 (2010).
5. H. Galarraga, D. A. Lados, R. R. Dehoff, M. M. Kirka, and P. Nandwana, Additive Manufact. **10**, 47–57 (2016).
6. S. M. Ahmadi et.al, Journal of the Mechanical Behavior of Biomedical Materials **34**, 106–115 (2014).
7. A. I. Golodnov, Yu .N. Loginov, and S. I. Stepanov, Solid State Phenomena **284**, 380–385 (2018).
8. S. I. Stepanov, Yu. N. Loginov, V. P. Kuznetsov, and A. A. Popov, Metal Sci. and Heat Treatment **60**, 315–321 (2018).
9. G. Kasperovich and J. Hausmann, Journal of Materials Processing Technology **220**, 202–214 (2015).
10. M. Simonelli, Y. Y. Tse, C. Tuck, Materials Science and Engineering: A **616**, 1–11 (2014).
11. M. Simonelli, Y. Y. Tse, C. Tuck, Materials Science and Engineering: A **616**, 1–11 (2014).